Conical Intersections in Thymine

Serhiy Perun and Andrzej L. Sobolewski*

Institute of Physics, Polish Academy of Sciences, PL-02668 Warsaw, Poland

Wolfgang Domcke

Department of Chemistry, Technical University of Munich, D-85747 Garching, Germany

Received: June 1, 2006; In Final Form: September 20, 2006

The mechanisms which are responsible for the radiationless deactivation of the $n\pi^*$ and $\pi\pi^*$ excited singlet states of thymine have been investigated with multireference ab initio methods (the complete-active-space self-consistent-field (CASSCF) method and second-order perturbation theory with respect to the CASSCF reference (CASPT2)) as well as with the CC2 (approximated singles and doubles coupled-cluster) method. The vertical excitation energies, the equilibrium geometries of the $^1n\pi^*$ and $^1\pi\pi^*$ states, as well as their adiabatic excitation energies have been determined. Three conical intersections of the S_1 and S_0 energy surfaces have been located. The energy profiles of the excited states and the ground state have been calculated with the CASSCF method along straight-line reaction paths leading from the ground-state equilibrium geometry to the conical intersections. All three conical intersections are characterized by strongly out-of-plane distorted geometries. The lowest-energy conical intersection (CI_1) arises from a crossing of the lowest $^1\pi\pi^*$ state with the electronic ground state. It is found to be accessible in a barrierless manner from the minimum of the $^1\pi\pi^*$ state, providing a direct and fast pathway for the quenching of the population of the lowest optically allowed excited states of thymine. This result explains the complete diffuseness of the absorption spectrum of thymine in supersonic jets. The lowest vibronic levels of the optically nearly dark $^1n\pi^*$ state are predicted to lie below CI_1, explaining the experimental observation of a long-lived population of dark excited states in gas-phase thymine.

1. Introduction

The nucleic acid bases are the main chromophores of DNA and absorb strongly in the 200−300 nm range. Nevertheless, the quantum yields of photoproducts involving isomerization of the heteroaromatic rings are very low.[1] It seems that photochemical reactions are efficiently quenched in DNA by ultrafast nonradiative decay processes back to the electronic ground state. These nonradiative excited-state deactivation mechanisms provide DNA with a high degree of intrinsic photostability.[2]

Experimental and computational work in recent years has led to considerable progress in the understanding of the mechanisms of radiationless decay of the isolated DNA bases adenine (A), cytosine (C), guanine (G), and thymine (T), as well as the RNA base uracil (U). Resonance-enhanced multiphoton ionization (REMPI) as well as laser-induced fluorescence (LIF) spectra taken in supersonic jets have been found to be broad and structureless in uracil and thymine, indicating extensive mixing among excited states and/or ultrashort excited-state lifetimes[3]. For adenine, guanine, and cytosine, on the other hand, sharp excitation spectra indicating long-lived vibronic levels have been observed, albeit only in a narrow energy interval above the origin of the spectra.[4−7] Time-resolved measurements in solution[8−12] as well as in the gas phase[13−16] have confirmed the very short (subpicosecond) excited-state lifetimes of the DNA bases. Computational studies have revealed the existence of low-lying conical intersections as well as low-barrier reaction paths leading to the latter.[17−28] On the basis of the computationally identified pathways, it has become possible to develop a simple mechanistic picture of the photophysics of isolated nucleic acid bases, in which ultrafast internal conversion dynamics at conical intersections[29] plays a decisive role. It has been proposed that conical intersections related to specific out-of-plane deformations of the six-membered heteroaromatic rings dominate the radiationless deactivation of the lowest excited states of A,[21−24,27,28] U,[20,25,26] and C.[17,19] For adenine, it has been shown that conical intersections related to excited-state hydrogen abstraction from acidic groups[18,22−24] and opening of the five-membered ring[22] become accessible at higher excitation energies (≈5.5 eV). Taken together, these radiationless-decay processes via conical intersections seem to provide the DNA bases with a high degree of photostability over a wide range of UV wavelengths.

Relatively few computational investigations of the excited states have been published for T. Vertical excitation energies have been obtained by Lorentzon et al., Shukla and Mishra as well as Shukla and Leszczynski with the CASPT2 method (second-order perturbation theory based on the complete-active-space self-consistent-field (CASSCF) reference), the single-excitation configuration interaction (CIS) method, and time-dependent density functional theory (TDDFT), respectively.[30−32] Geometry optimization at the CIS level has predicted significantly nonplanar geometries of the lowest $^1n\pi^*$ and $^1\pi\pi^*$ excited states of T.[31] More recently, Gustavsson et al. have performed a more extensive exploration of the excited-state potential-energy surfaces of T and U with CASSCF and TDDFT

* To whom correspondence should be addressed. E-mail: sobola@ifpan.edu.pl.

10.1021/jp0633897 CCC: $33.50
Published on Web 11/18/2006

methods.[26] A S_1-S_0 conical intersection has been located at the CASSCF level which is reached by a pronounced torsion of the C_4-C_5 bond and pyramidization at C_5, in agreement with previous results for U.[20] A barrier of about 0.2 eV (1600 cm^{-1}) has been predicted on the reaction path between the S_1 minimum and the conical intersection in aqueous solution (solvation has been described in a dielectric continuum model).

In the present work, we have employed the CASSCF/CASPT2[33] as well as CC2 (approximated second-order singles and doubles coupled-cluster)[34] methods for the characterization of the potential-energy surfaces of the lowest excited singlet states of T.

2. Computational Methods

The ground-state geometry of T has been determined with the MP2 (second-order Møller−Plesset) method, making use of the resolution-of-identity (RI) approximation.[35] The correlation-consistent polarized valence double-ζ (cc-pVDZ) basis set[36] with polarization functions on all atoms was used in the MP2 ground-state geometry optimization.

Vertical excitation energies have been calculated with the CASSCF/CASPT2[33] and CC2[34] methods. A systematic study of the influence of the quality of the basis set on the excitation energies has been performed. The following four basis sets have been employed (number of primitives/basis functions in parentheses): def-SV(P) (240/138),[37] cc-pVDZ (348/156),[36] ANO-L (669/156),[38] and TZVPP (510/ 363).[39]

The search for the minimum-energy structures of the lowest $^1\pi\pi^*$ and $^1n\pi^*$ states was performed with the CASSCF and CC2 methods. In a first step, the geometries have been optimized with C_s symmetry constraint. This is useful to distinguish between a″(π) and a′(σ/n) orbitals and to divide the electronically excited states into A′ and A″ symmetry blocks. Taking the local minimum-energy structures of the $^1\pi\pi^*$ and $^1n\pi^*$ states obtained with C_s-constrained optimization as initial guesses, we have reoptimized the geometries of the excited states in C_1 symmetry. The active space in these CASSCF/CASPT2 calculations consisted of 12 electrons distributed over 10 ($8\pi + 2n$) valence orbitals.

The search for conical intersections between the S_1 and S_0 energy surfaces was performed at the CASSCF level, using the corresponding module in the Gaussian 98 program package.[40,41] The active space in this case was reduced to six electrons distributed over six orbitals. The initial guesses of the geometries of the conical intersections were constructed by stretching and twisting of the C−N bonds of the heteroaromatic ring of T, as suggested by previous results for DNA bases.[19−28] These previous calculations have shown that the S_0 and S_1 wave functions at the S_1-S_0 conical intersections typically are of biradical character and are well represented by a rather compact active space. This justifies the use of the small 6/6 active space for the location of the conical intersections. The Cartesian coordinates of all optimized structures are given in the Supporting Information.

Having optimized the local minima of the excited states and the conical intersections, the linearly interpolated internal-coordinate (LIIC) reaction path was constructed. The LIIC path is defined as the straight line in the multidimensional internal-coordinate space which connects a given initial structure (local minimum) with a given final structure (conical intersection). Single-point energy calculations have been performed along each LIIC path with the state-averaged CASSCF method to obtain the reaction-path potential-energy profiles. For these single-point energy calculations, the larger active space consisting of 12 electrons distributed over 10 ($8\pi + 2n$) orbitals has been used. The six lowest electronic states were included in the CASSCF energy functional with equal weights. The continuity of the electronic character of the excited states along the reaction path was controlled by the calculation of the transition dipole moments (from the ground state to the corresponding excited state) as well as by the analysis of the configurational character of the CASSCF wave functions. Finally, single-point energy calculations were performed at the optimized ground-state geometry as well as at the excited-state local minima and conical-intersection structures with the CASPT2 and CC2 methods, employing the cc-pVDZ basis set.

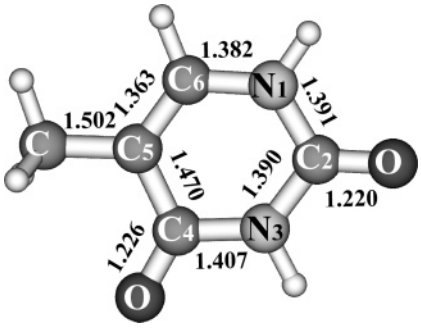

Figure 1. Ground-state equilibrium geometry of thymine, determined at the MP2/cc-pVDZ level. Bond lengths are given in angstroms. Standard numeration of the atoms is given here and in what follows. The numeration of hydrogen atoms corresponds to that of the heavy atoms involved in the respective covalent bonds.

The TURBOMOLE−5.7 package[42] was used for all MP2 and CC2 calculations. The CASSCF optimization of the excited-state equilibrium structures was performed with the GAMESS[43] package, while the CASSCF/CASPT2 single-point energy calculations were performed with the MOLCAS-5 program suite.[44]

3. Results and Discussion

3.1. Ground-state Geometry and Vertical Excitation Energies. The ground-state equilibrium geometry of T determined at the MP2/cc-pVDZ level is shown in Figure 1. This structure belongs to the C_s symmetry group. All atoms, with the exception of two hydrogens of the methyl group, lie in the plane of the six-membered ring. The calculated dipole moment is 3.84 D.

The vertical excitation energies of the lowest five excited singlet states of $^1\pi\pi^*$ and $^1n\pi^*$ character of T, obtained at the CASSCF, CASPT2, and CC2 levels with the four basis sets, are given in Table 1 ($^1\pi\pi^*$ states) and Table 2 ($^1n\pi^*$ states). As can be seen from Table 1, the CASSCF $^1\pi\pi^*$ excitation energies computed with the ANO-L basis set are lower than those calculated with the cc-pVDZ basis by about 0.3 eV. This average difference becomes about 0.2 eV at the CASPT2 level. The extension of the basis from cc-pVDZ to ANO-L lowers the CASSCF $^1n\pi^*$ energies by about 0.1 eV (see Table 2). At the CASPT2 level, on the other hand, the energies of the first two $^1n\pi^*$ transitions determined with the cc-pVDZ basis are lower than the corresponding ANO-L values by about 0.05 eV. Overall, the $^1\pi\pi^*$ excitation energies are more basis-set dependent than the $^1n\pi^*$ excitation energies.

The present CASPT2 results for the $^1\pi\pi^*$ states of T are in good agreement with the CASPT2 data reported previously by Lorentzon et al.[30] For the $^1n\pi^*$ states, on the other hand, we invariably obtained excitation energies which are higher by several tenths of an electronvolt than the data reported by Lorentzon et al. Neither extension of the active space (by

TABLE 1: Vertical Excitation Energies (in electronvolts) of the $^1\pi\pi^*$ States of Thymine, Computed with the CASSCF, CASPT2, and CC2 Methods Using the def-SV(P), cc-pVDZ, ANO-L, and TZVPP Basis Sets, at the MP2/cc-pVDZ Ground-state Geometry

	E(CASSCF)		*E*(CASPT2)		*E*(CC2)			
	cc-pVDZ	ANO-L	cc-pVDZ	ANO-L	def-SV(P)	cc-pVDZ	TZVPP	absorption in the gas phase [50]
$^1\pi\pi^*_1$	6.47	6.16	4.81	4.68	5.60	5.52	5.29	4.8
$^1\pi\pi^*_2$	7.24	7.06	5.99	5.84	6.70	6.59	6.39	5.7
$^1\pi\pi^*_3$	8.23	7.87	6.26	6.06	7.08	7.03	6.71	6.2
$^1\pi\pi^*_4$	9.19	8.83	7.08	6.80	7.99	7.92	7.56	>6.7
$^1\pi\pi^*_5$	9.35	9.26	7.99	7.79	8.37	8.15	7.70	

TABLE 2: Vertical Excitation Energies (in electronvolts) of the $^1n\pi^*$ States of Thymine, Computed with the CASSCF, CASPT2, and CC2 Methods Using the def-SV(P), cc-pVDZ, ANO-L, and TZVPP Basis Sets, at the MP2/cc-pVDZ Ground-state Geometry

	E(CASSCF)		*E*(CASPT2)		*E*(CC2)		
	cc-pVDZ	ANO-L	cc-pVDZ	ANO-L	def-SV(P)	cc-pVDZ	TZVPP
$^1n\pi^*_1$	5.05	4.95	4.97	5.02	5.06	5.00	4.88
$^1n\pi^*_2$	6.62	6.44	6.51	6.55	6.47	6.40	6.25
$^1n\pi^*_3$	8.09	8.01	7.32	7.29	6.93	6.85	6.64
$^1n\pi^*_4$	8.28	8.09	7.05	6.95	7.34	7.16	6.74
$^1n\pi^*_5$	10.4	10.3	8.56	8.44	7.35	7.30	7.11

additional *n* orbitals) nor the addition of diffuse functions has led to a significant lowering of the $^1n\pi^*$ excitation energies. It seems that the $^1n\pi^*$ excitation energies of Lorentzon et al. cannot be reproduced with standard basis sets and active spaces (Lorentzon et al. employed a special procedure of including diffuse functions in the basis set and subsequently deleting Rydberg-type orbitals from the active space).

In the case of the CC2 method, the $^1\pi\pi^*$ transition energies obtained with the TZVPP basis are lower than those computed with the def-SV(P) (cc-pVDZ) basis set by about 0.3 eV (0.2 eV) (see Table 1). For the $^1n\pi^*$ transitions, an average difference of about 0.2 eV is observed between the TZVPP and def-SV-(P) results. This difference is reduced to 0.15 eV (on average) for the TZVPP and cc-pVDZ results (see Table 2). The energies of higher transitions, both of $^1\pi\pi^*$ or $^1n\pi^*$ character, are more sensitive to the improvement of the basis set than those of the low-lying excited states. This reflects the increasingly ionic character of higher excited states and the onset of valence−Rydberg mixing.

Comparing the CASPT2 and CC2 excitation energies calculated with the cc-pVDZ basis set, we observe that the CC2 values for the $^1\pi\pi^*$ states are higher than the CASPT2 data by about 0.7 eV. For the $^1n\pi^*$ states, on the other hand, the CASPT2 and CC2 excitation energies obtained with the cc-pVDZ basis are very similar. Both the CC2 and CASPT2 excitation energies of the $^1\pi\pi^*$ states decrease with the extension of the basis set. The CC2 excitation energies are intrinsically higher than the experimental excitation energies and approach the latter from above with the extension of the basis set. The CASPT2 excitation energies of the $^1\pi\pi^*$ states, on the other hand, tend to be lower than the experimental values when large basis sets are employed. This feature of CASPT2 explains why often very accurate $^1\pi\pi^*$ excitation energies are predicted with basis sets of DZP quality.

Comparison with (estimated) experimental gas-phase vertical excitation energies is possible for the optically allowed $^1\pi\pi^*$ states; see Table 1. The CASPT2 excitation energies obtained with the ANO-L basis are in very good agreement with the experimental estimates (within 0.1 eV). The CC2 excitation energies obtained with the TZVPP basis appear to be too high in energy by about 0.5 eV.

3.2. Excited-state Minimum-energy Structures and Energetics. The equilibrium geometries of the lowest $^1n\pi^*$ and $^1\pi\pi^*$ excited states of T, optimized at the CC2/cc-pVDZ level with C_s symmetry constraint, are shown in Figure 2. The bond lengths (in angstroms) are indicated. The bond lengths determined at the CASSCF/cc-pVDZ level are given in parentheses. Most bond lengths agree within a precision of about 0.05 Å. In the case of the $^1n\pi^*$ equilibrium structure (Figure 2a), however, the length of the $C_4{=}O_4$ bond predicted by CC2 is longer (by 0.1 Å) and the length of the $C_4{-}C_5$ is shorter (by 0.093 Å) than the corresponding distances determined at the CASSCF level. In the case of the $^1\pi\pi^*$ equilibrium geometry (Figure 2b), differences of about 0.1 Å (0.074 Å) are found between the CC2 and CASSCF lengths of the $N_1{-}C_2$ ($C_2{=}O_2$) bonds.

The lengths of the $C_4{=}O_4$ and $C_4{-}C_5$ bonds of the $^1n\pi^*$ equilibrium structure differ substantially from those of the ground state (see Figure 1). Since the *n* orbital of the lowest $^1n\pi^*$ excited state is primarily of O_4 lone-pair character, excitation to this state leads to a shift of electronic population toward the aromatic ring, resulting in a considerable change of the geometry of the $C_5{-}C_4{=}O_4$ moiety. The previously reported equilibrium geometry of the $^1n\pi^*$ excited state of T determined at the CIS level[30] as well as the MRCI[20] and DFT/MRCI[45] optimized $^1n\pi^*$ minimum-energy structures of U are also characterized by an elongated $C_4{=}O_4$ distance of about 1.3 Å. The CC2 method predicts a substantially longer $C_4{=}O_4$ bond distance of 1.44 Å. This substantial elongation of the $C_4{=}O_4$ bond can be considered as a characteristic property of the lowest $^1n\pi^*$ state of T and U. The CC2-determined equilibrium geometry of the $^1\pi\pi^*$ excited state is characterized by a moderate extension of the bond lengths in comparison with the ground-state structure. The increase of the $C_5{=}C_6$ distance by about 0.1 Å indicates a certain change of character of this bond from a double bond toward a single bond.

Optimization of the $^1n\pi^*$ excited-state geometry without symmetry constraint, either on the CC2 or the CASSCF level, leads to a slightly out-of-plane distorted structure. The distortion involves primarily the $C_5C_4N_3$ moiety. The dihedral angles which characterize this distortion are $\delta(C_5C_4N_3C_2) = 9.4°$ and $\delta(C_5C_4N_3H) = 165.9°$ at the CASSCF level. The CC2 method predicts a qualitatively similar slightly nonplanar structure, with dihedral angles $\delta(C_5C_4N_3C_2) = 6.02°$ and $\delta(C_5C_4N_3H) = 170.4°$. All attempts of optimization of the $^1\pi\pi^*$ equilibrium geometry without symmetry constraints at the CC2 level have failed, resulting in the collapse of the $^1\pi\pi^*$ wave function to that of the $^1n\pi^*$ excited state. However, it was possible to optimize the $^1\pi\pi^*$ minimum-energy structure without symmetry

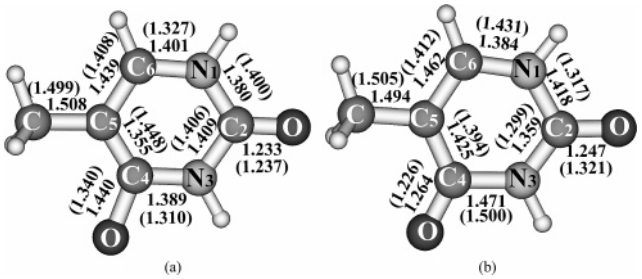

Figure 2. Equilibrium geometries of the lowest $^1n\pi^*$ (a) and $^1\pi\pi^*$ (b) excited states of thymine, determined at the CC2/cc-pVDZ level with C_s symmetry constraint. Bond lengths are given in angstroms. The bond lengths determined at the CASSCF/cc-pVDZ level are given in parentheses.

constraints with the CASSCF method. The resulting geometry is characterized by a slightly puckered $C_4C_5C_6$ moiety, with the relevant dihedral angles being $\delta(C_4C_5C_6N_1) = 5.32°$ and $\delta(C_4C_5C_6H) = -156.6°$.

The adiabatic excitation energies of the $^1\pi\pi^*$ and $^1n\pi^*$ excited states, calculated at the CC2/cc-pVDZ and CASPT2/cc-pVDZ levels at the CASSCF and CC2 optimized planar excited-state equilibrium geometries, are given in Table 3. Optimization of the geometry at the CC2 level stabilizes the energy of the $^1\pi\pi^*$ excited state by 0.5 eV, while the energy of the $^1n\pi^*$ excited state is lowered by 1.05 eV. For comparison, CASPT2 single-point energy calculations were performed at the CC2-optimized geometries of both excited states. Inclusion of dynamic electron correlation in the geometry optimization leads to an adiabatic excitation energy of the $^1\pi\pi^*$ state of 4.48 eV and that of the $^1n\pi^*$ excited state of 4.29 eV.

It can be seen that the CASPT2 adiabatic excitation energies, calculated with CASSCF and CC2 optimized geometries, respectively, may differ by several tenths of an electronvolt. This reflects a long-standing problem of the CASSCF/CASPT2 protocol: the neglect of dynamical electron correlation effects in the geometry optimization is a serious approximation. For a recent discussion of this problem, see ref 46. An example of these difficulties is provided by the vertical and adiabatic excitation energies of the lowest $^1\pi\pi^*$ state in Tables 1 and 3. The adiabatic excitation energy calculated with CASPT2 for the CASSCF-optimized excited-state geometry is higher than the vertical excitation energy calculated with CASPT2 at the MP2-optimized geometry of the ground state. Obviously, the MP2 ground-state equilibrium geometry is a better approximation to the true (that is, CASPT2) excited-state geometry than the CASSCF-optimized geometry of the excited state. This artifact disappears when CC2-optimized excited-state geometries are used (see Table 3). The combination of CC2 geometry optimization and CASPT2 single-point energy calculation thus appears to be a potentially very useful improvement of the CASSCF/CASPT2 protocol.

As mentioned above, the breaking of the C_s symmetry leads to slightly puckered structures of the $^1n\pi^*$ and $^1\pi\pi^*$ excited states. The associated stabilization energy is 0.12 eV for the $^1\pi\pi^*$ excited state (resulting in an adiabatic excitation energy of 4.36 eV) and 0.43 eV for the $^1n\pi^*$ state (resulting in an adiabatic excitation energy of 3.87 eV) at the CASPT2 level. For comparison, the estimated origin of the $^1\pi\pi^*$ absorption spectrum of jet-cooled T is at 4.39 eV.[3] This again confirms that CASPT2 yields very accurate excitation energies for the lowest $^1\pi\pi^*$ state.

3.3. Conical Intersections. The optimization of the geometries of conical intersections of the S_0 and S_1 energy surfaces was performed at the CASSCF level with the cc-pVDZ basis set. Three different structures, representing local minima of the hypersurface of S_1-S_0 intersection, were found. These structures are shown in Figure 3. We refer to them as CI_1, CI_2, and CI_3 in what follows. All structures are strongly out-of-plane distorted, involving pronounced torsion of the C_4-C_5 bond and/or pyramidization at C_5. The lengths of the C_4-C_5 and C_5-C_6 bonds of all three conical-intersection geometries differ significantly from those of the ground-state structure as well as the $^1n\pi^*$ and $^1\pi\pi^*$ excited-state structures.

TABLE 3: CASPT2/cc-pVDZ and CC2/cc-pVDZ Adiabatic Excitation Energies (in electronvolts) of the Lowest $^1\pi\pi^*$ and $^1n\pi^*$ States of Thymine, Calculated at the CASSCF and CC2 Optimized Planar Excited-state Geometries

method/ excited state	CASPT2		CC2	
method of geometry optimization	$^1\pi\pi^*$	$^1n\pi^*$	$^1\pi\pi^*$	$^1n\pi^*$
CASSCF	5.23	4.69	5.30	4.65
CCS	4.48	4.29	5.02	3.95

The geometry of the CI_1 conical intersection (Figure 3a) is very similar to that reported by Gustavsson et al.[26] The methyl group is strongly out-of-plane displaced. The corresponding dihedral angle $\delta(N_3C_4C_5C)$ is 83.8°, and the $C-C_5$ bond is almost perfectly perpendicular to the ring plane. The two other dihedral angles, which are characteristic for the out-of-plane displacement of the H_6 atom and for the torsion of the C_5-C_6 bond, are $\delta(C_2N_1C_6H) = 147.7°$ and $\delta(C_4C_5C_6N_1) = 49.3°$, respectively. The value of the latter angle is in qualitative agreement with the magnitude of double-bond twisting of about 60°, which has been found to be typical for conical-intersection structures of DNA bases.[21] The CI_1 geometry does not exhibit an extended $C_4=O_4$ bond length. This is an indication that the character of the S_1 state at the crossing is $^1\pi\pi^*$ rather than $^1n\pi^*$.

As can be seen from Figure 3b, the CI_2 conical-intersection structure is, in addition to the out-of-plane displacement of the methyl group and the H_6 atom, characterized by a very pronounced out-of-plane distortion of the $C_4=O_4$ group. The length of the $C_4=O_4$ bond is 1.382 Å, considerably longer than in the ground state, indicating that the S_1 state is of $^1n\pi^*$ character at the intersection. The twisted C_4-C_5 bond is considerably longer than in the ground state. The dihedral angles characterizing the out-of-plane displacement of H_6 and the methyl group are $\delta(C_2N_1C_6H) = 69.5°$ and $\delta(N_3C_4C_5C) = 143.8°$, respectively. The dihedral angle $\delta(C_4C_5C_6N_1)$, which describes the twisting of the $C_5=C_6$ double bond, is 46.7°. The geometry of CI_2 resembles to a great extent the structure of the three-state ($S_0-S_1-S_2$) conical intersection determined by Matsika at the MRCI level for uracil.[45]

In the CI_3 structure (Figure 3c), two bond distances are strongly elongated: the length of the C_5-C_6 bond has increased to 1.552 Å and the $C_4=O_4$ bond has lengthened to 1.676 Å. The pronounced increase of the $C_4=O_4$ bond length is a clear indication that CI_3 corresponds to a crossing of the $^1n\pi^*$ state with the ground state. The dihedral angle $\delta(C_4C_5C_6N_1)$, which is a measure of the twisting of the $C_5=C_6$ bond, is 71.5° in the CI_3 structure, confirming the empirical rule mentioned above. The dihedral angles describing the out-of-plane displacements of the H_6 atom and the methyl group are $\delta(C_2N_1C_6H_6) = 99.2°$ and $\delta(N_3C_4C_5C) = 167.2°$.

To explore the correlation of the S_1-S_0 conical intersections with the vertically excited states, the LIIC reaction paths were constructed from the equilibrium geometry of the ground state to the corresponding conical-intersection structures. The CASSCF potential-energy profiles calculated along these paths are shown in Figure 4. It should be stressed that these LIIC/CASSCF energy functions are intended to give a qualitative overview of

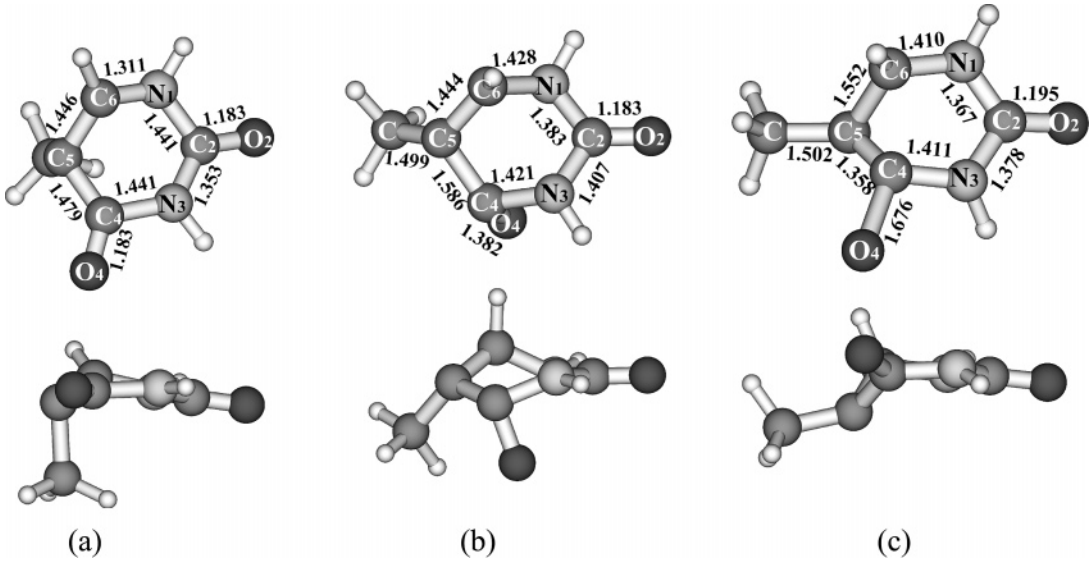

Figure 3. Geometries of the S_1-S_0 conical intersections CI_1 (a), CI_2 (b) and CI_3 (c) (top and side view), optimized at the CASSCF/cc-pVDZ level. Bond lengths are given in angstroms.

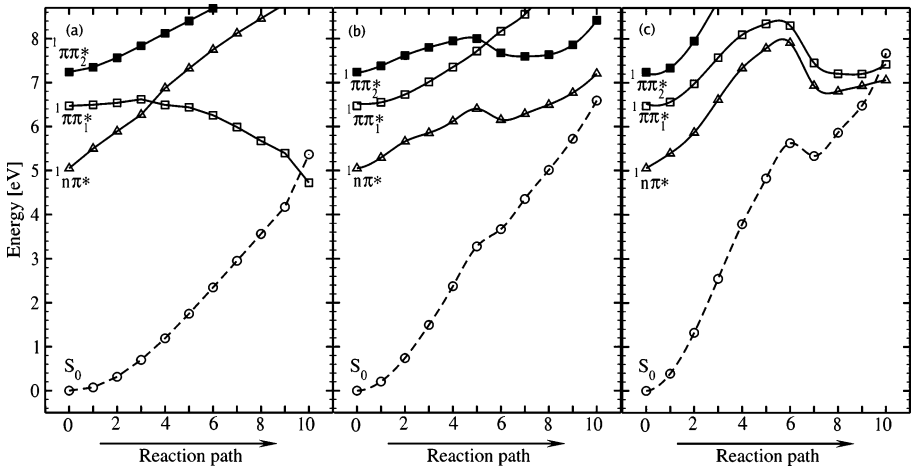

Figure 4. Potential-energy profiles of the ground state (circles), the $^1n\pi^*$ state (triangles), and the first (open squares) and the second (full squares) $^1\pi\pi^*$ states of thymine, calculated at the CASSCF/cc-pVDZ level along the LIIC reaction paths from the equilibrium geometry of the ground state to the CI_1 (a), CI_2 (b), and CI_3 (c) conical intersections. Eleven single-point energies have been calculated for each state along each path.

the diabatic state correlations. They do not provide quantitative energetic information, because (i) the reaction paths are not minimum-energy paths and (ii) dynamical electron-correlation effects are not included.

The calculated potential-energy profiles of the four states of interest along the reaction path from the minimum of the ground state to the CI_1 intersections are shown in Figure 4a. While the energies of the $^1n\pi^*$ excited state and the second $^1\pi\pi^*$ excited state increase monotonically along this reaction path, the energy profile of the lowest $^1\pi\pi^*$ excited state exhibits sort of a plateau at the beginning of the reaction path and then decreases, eventually crossing the energy profile of the ground state. The energy of this S_1-S_0 crossing is lower than the vertical excitation energies of the $^1n\pi^*$ state and the lowest $^1\pi\pi^*$ state. The energy functions of the $^1\pi\pi^*$ state and the $^1n\pi^*$ state cross at an energy which is only slightly above the $^1\pi\pi^*$ vertical excitation energy. While the CASSCF energy profiles in Figure 4a indicate the existence of a tiny barrier in the $^1\pi\pi^*$ energy profile, this barrier certainly will disappear when the minimum-energy reaction path is considered and dynamical electron-correlation effects are included. We can thus conclude that the lowest $^1\pi\pi^*$ state of T is connected in a barrierless manner with the S_1-S_0 conical intersection CI_1, which is the lowest-energy intersection identified in the present work. It should be mentioned that the reactive character of the $^1\pi\pi^*$ surface was noted previously for U.[20,25,31] The CI_1 intersection in T appears to be closely analogous to the conical intersection previously located in U.

As shown by Figure 4b, the conical intersection CI_2 arises from a degeneracy of the lowest $^1n\pi^*$ state with the ground state at an energy of about 7 eV. The gap of about 0.4 eV between the two states at the location of the conical intersection is of technical origin: the structure of the conical intersection has been determined with a smaller active space than that used for the single-point energy calculations along the LIIC path. The energy of CI_2 is about the same as the $^1\pi\pi^*$ vertical excitation energy. In contrast to CI_1, the energies of all excited states increase along the reaction path from the ground-state geometry to the CI_2 intersection.

Following the reaction path to the CI_3 intersection (Figure 4c), the energies of the lowest excited singlet states (the $^1n\pi^*$ state and the two $^1\pi\pi^*$ states) increase in a nonmonotonic fashion. The hump in all four potential-energy profiles probably is a feature introduced by the LIIC path: the straight-line path cuts through a ridge of the surfaces, rather than following the valley. A crossing of the lowest two excited states with the

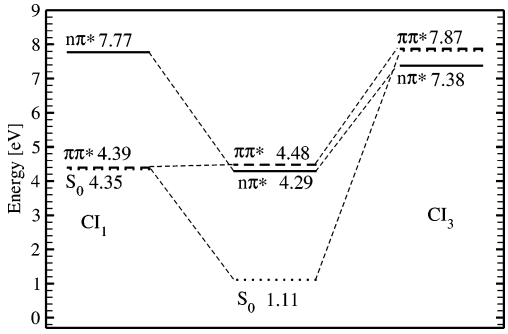

Figure 5. Energy-level diagram of the S_0 (dotted line), the $^1n\pi^*$ (solid line), and the $^1\pi\pi^*$ (dashed line) states of thymine, calculated with the CASPT2 method at the equilibrium geometry of the $^1n\pi^*$ excited state and the CI_1 and CI_3 conical intersections. The energies (relative to the minimum energy of the ground state) are given in electronvolts.

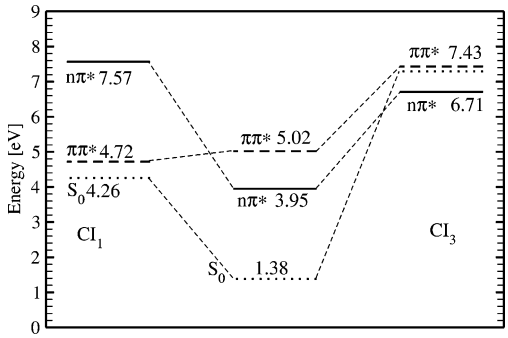

Figure 6. Energy-level diagram of the S_0 (dotted line), the $^1n\pi^*$ (solid line), and the $^1\pi\pi^*$ (dashed line) states of thymine, calculated with the CC2 method at the equilibrium geometry of the $^1n\pi^*$ excited state and the CI_1 and CI_3 conical intersections. The energies (relative to the minimum energy of the ground state) are given in electronvolts.

ground state is found at an energy of about 7 eV, which is higher than the $^1n\pi^*$ and $^1\pi\pi^*$ vertical excitation energies by 2.0 and 0.5 eV, respectively. The CI_3 structure exhibits a considerably elongated $C_4{=}O_4$ bond, reflecting the $^1n\pi^*$ character of the S_1 state at the crossing with the S_0 state. The lowest $^1\pi\pi^*$ state is very close in energy to the $^1n\pi^*$ and S_0 states at the crossing geometry of the latter, so that all three states become almost degenerate. This suggests that a three-state conical intersection can be found nearby. The existence of such intersections recently has been discussed for U[45] and C.[47]

Our final results on the energetics of the lowest singlet states of T are shown in Figures 5 and 6. In Figure 5, the energy-level diagram of the lowest $^1n\pi^*$ and $^1\pi\pi^*$ excited states and of the ground state is given, calculated at the planar equilibrium geometries of the $^1n\pi^*$ and $^1\pi\pi^*$ states and at the optimized CI_1, CI_3 structures with the CASPT2 method. The energy levels of CI_2 are not included for clarity (they are similar to those of CI_3). Figure 6 gives the corresponding results obtained with the CC2 method. As can be seen, the qualitative picture of the energetics of excited-state minima and conical intersections predicted by the two electronic-structure methods is quite similar. Both CASPT2 and CC2 predict that the CI_1 intersection is significantly lower than CI_2 and CI_3 and is energetically close to the minimum energies of the $^1n\pi^*$ and $^1\pi\pi^*$ excited states. The CASPT2 method predicts the energy of CI_1 about 0.1 eV higher than the minimum energy of the $^1n\pi^*$ excited state and about 0.1 eV lower than the minimum energy of the $^1\pi\pi^*$ state. When the CC2 method is employed, these differences increase to about $\pm$ 0.3 eV. According to both CASPT2 and CC2, the CI_3 and CI_2 conical intersections occur at energy of about 7.5 eV. This is about 3 eV higher than the minimum energies of the $^1\pi\pi^*$ and $^1n\pi^*$ excited states. We thus can conclude that the CI_2 and CI_3 conical intersections lie too high in energy to be involved in the photophysics of the lowest excited states of T.

3.4. Discussion. Canuel et al. have observed a two-component decay of T in the gas phase with lifetimes of 105 fs and 5.12 ps, respectively.[16] In light of the present results, the shorter component can be interpreted as the decay of the $^1\pi\pi^*$ excited state through the CI_1 conical intersection, while the longer time scale may reflect the decay of low vibronic levels of the $^1n\pi^*$ excited state. According to He et al., the excitation of T to the S_1 state in the gas phase results in a partial trapping of the molecule in a dark state, which was suggested to be of $^1n\pi^*$ character.[15,48] The lifetime of this dark state was determined to be of the order of tens to hundreds of nanoseconds. The excited-state landscape described above seems to confirm the model proposed in ref 47. The efficiency of the decay of the $^1n\pi^*$ state depends on the relative energy of the $^1n\pi^*$ origin and the CI_1 conical intersection, as well as on the height of the barrier which separates the $^1n\pi^*$ minimum from CI_1 (if such a barrier exists at all). According to the calculations, the $^1n\pi^*$ origin is located slightly below the lowest S_1-S_0 conical intersection in T, which supports the idea of a long-lived population of dark vibronic levels (close to the local minimum of the $S_1(n\pi^*)$ surface). All our attempts of locating a saddle point on the S_1 potential-energy surface were unsuccessful. The origin of the lowest $^1\pi\pi^*$ state, on the other hand, is predicted above the energy of the lowest S_1-S_0 conical intersection. This result, together with the absence of a barrier on the reaction path to CI_1, indicates a rapid radiationless decay of all $^1\pi\pi^*$ vibronic energy levels through this conical intersection, in agreement with the observation of a completely structureless excitation spectrum of T in supersonic jets.[3]

It should be mentioned that the model presented here is based on the qualitative analysis of the character of the potential-energy surfaces of the lowest excited states of T. The development of a more precise picture of the dynamics of T upon electronic excitation, which involves the competition of various radiationless electronic decay channels with intrastate vibrational relaxation, requires time-dependent quantum wave packet calculations on accurate multidimensional potential-energy surfaces.

It should finally be pointed out that presence of a solvent may significantly alter the excited-state energetics of T.[26] It was estimated for uracil that solvation by six water molecules raises the energy of the $^1n\pi^*$ excited state by about 0.5 eV.[49] A similar effect is expected for thymine and may lead to a reversal of the ordering of the $^1n\pi^*$ and $^1\pi\pi^*$ excited states as well as to a change in the relative energy of the relevant conical intersections. Solvation may thus have a significant impact on the photophysical behavior of T. In ref 48, it has been shown that complexation with water molecules indeed leads to the disappearance of the signal associated with the long-lived dark state.

4. Conclusions

The energy surfaces of the excited singlet states of T have been explored with the CASSCF/CASPT2 and CC2 methods. Comparison of the CASPT2 and CC2 vertical excitation energies shows that both methods predict a qualitatively similar excitation spectrum, although there are differences in detail. The CC2 method with the basis sets employed in the present work tends to overestimate the energies of the $^1\pi\pi^*$ transitions, while CASPT2 yields $^1\pi\pi^*$ excitation energies in good agreement with

the experimental data. For the $^1n\pi^*$ states, the differences between CASPT2 and CC2 excitation energies are minor.

The equilibrium geometries of the lowest $^1n\pi^*$ and $^1\pi\pi^*$ excited states of T have been determined at the CASSCF and CC2 levels. They are slightly nonplanar. A significant increase of the $C_4{=}O_4$ bond length is characteristic for the $^1n\pi^*$ excited state. The energies of the lowest $^1n\pi^*$ and $^1\pi\pi^*$ excited states have been calculated with CC2 and CASPT2 at the CASSCF- and CC2-optimized geometries. The combination of CC2 geometry optimization and CASPT2 single-point energy calculation appears to be a viable alternative to the CASSCF/CASPT2 protocol.

Three $S_1{-}S_0$ conical intersections (more precisely, three local minima of the $S_1{-}S_0$ intersection hypersurface) have been located. All conical intersections are characterized by strongly out-of-plane distorted geometries of the heterocyclic ring. In particular, the H_6 atom and the methyl group are twisted out of the plane of the ring. The lowest-energy intersection, CI_1, arises from a crossing of the lowest $^1\pi\pi^*$ state with the S_0 state and is accessible in a barrierless manner from the minimum of the $^1\pi\pi^*$ state. It provides a direct and fast pathway for the quenching of the population of the lowest $^1\pi\pi^*$ excited state of T. This finding explains the absence of any sharp structures in the absorption spectrum of T in supersonic jets. The other two conical intersections, CI_1 and CI_2, involve the crossing of the lowest $^1n\pi^*$ excited state with the S_0 state and are higher in energy (about 7.5 eV above the S_0 minimum). They are presumably not relevant for the radiationless decay of the lowest excited states but may come into play when T is excited with larger excess energies.

Acknowledgment. This work has been supported by the Committee for Scientific Research of Poland (Grants Nos. 3T09A 160 28 and 3T09A 107 28), a travel grant of the Deutsche Forschungsgemeinschaft (for A.L.S.) as well as a travel grant of the COST action P9 (for S.P.).

Supporting Information Available: Tables showing the Cartesian coordinates of all optimized structures. This material is available free of charge via the Internet at http://pubs.acs.org.

References and Notes

(1) Cadet, J.; Vigny, P. In *Bioorganic Photochemistry*; Morrison, H., Ed.; Wiley: New York, 1990; Vol. 1, p 1.

(2) Crespo-Hernandez, C. E.; Cohen, B.; Hare, P. M.; Kohler, B. *Chem. Rev.* **2004**, *104*, 1977.

(3) Brady, B. B.; Peteanu, L. A.; Levy, D. H. *Chem. Phys. Lett.* **1988**, *147*, 538.

(4) Kim, N. J.; Jeong, G.; Kim, Y. S.; Sung, J.; Kim, S. K.; Park, Y. D. *J. Chem. Phys.* **2000**, *113*, 10051.

(5) Nir, E.; Kleinermanns, K.; Grace, L.; de Vries, M. S. *J. Phys. Chem. A* **2001**, *105*, 5106.

(6) Nir, E.; Plützer, C.; Kleinermanns, K.; de Vries, M. S. *Eur. Phys. J. D* **2002**, *20*, 317.

(7) Nir, E.; Kleinermanns, K.; de Vries, M. S. *Phys. Chem. Chem. Phys.* **2003**, *5*, 4780.

(8) Pecourt, J.-M. L.; Peon, J.; Kohler, B. *J. Am. Chem. Soc.* **2001**, *123*, 10370.

(9) Reuther, A.; Nikogosyan, D. N.; Laubereau, A. *J. Phys. Chem.* **1996**, *100*, 5570.

(10) Peon, J.; Zewail, A. H. *Chem. Phys. Lett.* **2001**, *348*, 255.

(11) Gustavsson, T.; Sharonov, A.; Markovitsi, D. *Chem. Phys. Lett.* **2002**, *351*, 195.

(12) Pancur, T.; Schwalb, N. K.; Renth, F.; Temps, F. *Chem. Phys.* **2005**, *313*, 199.

(13) Kang, H.; Lee, K. T.; Jung, B.; Ko, Y. J.; Kim, S. K. *J. Am. Chem. Soc.* **2002**, *124*, 12958.

(14) Ullrich, S.; Schultz, T.; Zgierski, M. Z.; Stolow, A. *Phys. Chem. Chem. Phys.* **2004**, *6*, 2796.

(15) He, Y.; Wu, C.; Kong, W. *J. Phys. Chem. A* **2003**, *107*, 5145.

(16) Canuel, C.; Mons, M.; Piuzzi, F.; Tardivel, B.; Dimicoli, L.; Elhanine, M. *J. Chem. Phys.* **2005**, *122*, 074316.

(17) Ismail, N.; Blancafort, L.; Olivucci, M.; Kohler, B.; Robb, M. A. *J. Am. Chem. Soc.* **2002**, *124*, 6818.

(18) Sobolewski, A. L.; Domcke, W. *Eur. Phys. J. D* **2002**, *20*, 369.

(19) Merchan, M.; Serrano-Andres, L. *J. Am. Chem. Soc.* **2003**, *125*, 8108.

(20) Matsika, S. *J. Phys. Chem. A* **2004**, *108*, 7584.

(21) Perun, S.; Sobolewski, A. L.; Domcke, W. *J. Am. Chem. Soc.* **2005**, *127*, 6257.

(22) Perun, S.; Sobolewski, A. L.; Domcke, W. *Chem. Phys.* **2005**, *313*, 107.

(23) Marian, C. M. *J. Chem. Phys.* **2005**, *122*, 104314.

(24) Bronstedt Nielsen, S.; Solling, T. I. *ChemPhysChem* **2005**, *6*, 1.

(25) Zgierski, M. Z.; Patchkovskii, S.; Fujiwara, T.; Lim, E. *J. Phys. Chem. A* **2005**, *109*, 9384.

(26) Gustavsson, T.; Bányász, Á.; Lazzaroto, E.; Markovitsi, D.; Scalmani, G.; Frisch, M. J.; Barone, V.; Improta, R. *J. Am. Chem. Soc.* **2006**, *128*, 607.

(27) Chen, H.; Li, S. *J. Phys. Chem. A* **2005**, *109*, 8443.

(28) Blancafort, L. *J. Am. Chem. Soc.* **2006**, *128*, 210.

(29) *Conical Intersections: Electronic Structure, Dynamics and Spectroscopy;* Domcke, W., Yarkony, D. R., Köppel, H., Eds.; World Scientific: Singapore, 2004.

(30) Lorentzon, J.; Fülscher, M. P.; Roos, B. O. *J. Am. Chem. Soc.* **1995**, *117*, 9265.

(31) Shukla, M. K.; Mishra, P. C. *Chem. Phys.* **1999**, *240*, 319.

(32) Shukla, M. K.; Leszczynski, J. *J. Comput. Chem.* **2004**, *25*, 768.

(33) Roos, B. O.; Andersson, K. *Chem. Phys. Lett.* **1995**, *245*, 215.

(34) Christiansen, O.; Koch, H.; Jørgensen, P. *Chem. Phys. Lett.* **1995**, *243*, 409.

(35) Weigend, F.; Häser, M. *Theor. Chem. Acc.* **1997**, *97*, 331.

(36) Dunning, T. H., Jr. *J. Chem. Phys.* **1989**, *90*, 1007.

(37) Schaefer, A.; Horn, H.; Ahlrichs, R. *J. Chem. Phys.* **1992**, *97*, 2571.

(38) Widmark, P.-O.; Malmqwist, P.-Å.; Roos, B. O. *Theor. Chim. Acta* **1990**, *77*, 291.

(39) Schaefer, A.; Huber, C.; Ahlrichs, R. *J. Chem. Phys.* **1994**, *100*, 5829.

(40) Bearpark, M. J.; Robb, M. A.; Schlegel, H. B. *Chem. Phys. Lett.* **1994**, *223*, 269.

(41) Frisch, M. J.; Trucks, G. W.; Schlegel, H. B.; Scuseria, G. E.; Robb, M. A.; Cheeseman, J. R.; Zakrzewski, V. G.; Montgomery, J. A., Jr.; Stratmann, R. E.; Burant, J. C.; Dapprich, S.; Millam, J. M.; Daniels, A. D.; Kudin, K. N.; Strain, M. C.; Farkas, O.; Tomasi, J.; Barone, V.; Cossi, M.; Cammi, R.; Mennucci, B.; Pomelli, C.; Adamo, C.; Clifford, S.; Ochterski, J.; Petersson, G. A.; Ayala, P. Y.; Cui, Q.; Morokuma, K.; Malick, D. K.; Rabuck, A. D.; Raghavachari, K.; Foresman, J. B.; Cioslowski, J.; Ortiz, J. V.; Baboul, A. G.; Stefanov, B. B.; Liu, G.; Liashenko, A.; Piskorz, P.; Komaromi, I.; Gomperts, R.; Martin, R. L.; Fox, D. J.; Keith, T.; Al-Laham, M. A.; Peng, C. Y.; Nanayakkara, A.; Gonzalez, C.; Challacombe, M.; Gill, P. M. W.; Johnson, B.; Chen, W.; Wong, M. W.; Gonzalez, J. L.; Head-Gordon, C. M.; Replogle, E. S.; Pople, J. A. *GAUSSIAN 98*; Gaussian Inc.: Pittsburgh, PA, 1998; see also http:// www.Gaussian.com.

(42) Ahlrichs, R.; Bär, M.; Häser, M.; Horn, H.; Kölmel, C. *Chem. Phys. Lett.* **1989**, *162*, 165; see also http://www.cosmologic.de.

(43) Schmidt, M. W.; Baldridge, K. K.; Boatz, J. A.; Elbert, S. T.; Gordon, M. S.; Jensen, J. H.; Koseki, S.; Matsunaga, M.; Nguyen, K. A.; Su, S. J.; Windus, T. L.; Dupuis, M.; Montgomery, J. A. *J. Comput. Chem.* **1993**, *14*, 1347; see also http://www.msg.ameslab.gov/GAMESS/.

(44) *MOLCAS*, version 5.2, Andersson, K.; Barysz, M.; Bernhardsson, A.; Blomberg, M. R. A.; Carissan, Y.; Cooper, D. L.; Cossi, M.; Devarajan, A.; Fülscher, M. P.; Gaenko, A.; Gagliardi, L.; de Graaf, C.; Hess, B. A.; Hagberg, D.; Karlström, G.; Krogh, J. W.; Lindh, R.; Malmqvist, P.-Å.; Nakajima, T.; Neogrády, P.; Olsen, J.; Pedersen, T. B.; Raab, J.; Roos, B. O.; Ryde, U.; Schimmelpfennig, B.; Schütz, M.; Seijo, L.; Serrano-Andrés, L.; Siegbahn, P. E. M.; Stålring, J.; Thorsteinsson, T.; Veryazov, V.; Widmark P.-O.; see also http://www.teokem.lu.se/molcas/.

(45) Matsika, S. *J. Phys. Chem. A* **2005**, *109*, 7538.

(46) Serrano-Andre, L.; Merchan, M. *THEOCHEM* **2005**, *729*, 99.

(47) Blancafort, L.; Robb, M. A. *J. Phys. Chem. A* **2004**, *108*, 10609.

(48) He, Y.; Wu, C.; Kong, W. *J. Phys. Chem. A* **2004**, *108*, 943.

(49) Marian, C. M.; Schneider, F.; Kleinschmidt, M.; Tatchen, J. *Eur. Phys. J. D* **2002**, *20*, 357.

(50) Clark, L. B.; Peschel, G. G.; Tinoco, I., Jr. *J. Mol. Biol.* **1962**, *4*, 500.